Structural Sizing for EDP Valve Body for HPHT Wellhead

João Victor Carvalho de Mattos[1*], Leonardo Marins Lúcio[1], Márcio de Melo Araújo[1], José Severino Fernandez Alvarez[1]

[1]SENAI CIMATEC University; Salvador, Bahia, Brazil

The reduction in production from active oil wells in Brazil and the depletion of reservoirs have driven research into deep-sea reservoirs, especially on the Brazilian equatorial margin and in projects such as Sergipe-Águas-Profundas. This work aims to design an EDP valve for intervention in HPHT (High Pressure, High Temperature) offshore wells. API and ASME standards, in addition to technical literature, were used to define the appropriate material and mechanical properties, and to calculate allowable stresses, as well as the stresses acting on the body and its components, using stress criterion to ensure equipment integrity. Stress concentrations were applied in regions with geometric alterations, as these are more critical. Finite element analysis more accurately assessed the equipment's behavior under the established conditions. Both calculation models were within the allowable design limits and demonstrate that the extreme conditions of HPHT wells require a thorough analysis of the design parameters.

Keywords: Oil and Gas. High-Pressure-High-Temperature. Intervention. Emergency Disconnect Package. Structural Analysis.

Brazil seeks to reduce oil imports and explore deep-water reservoirs, such as the projects of Sergipe Águas Profundas and the equatorial margin, aiming for self-sufficiency, due to their high production potencial [1,2]. Those projects must also align with current ecological demands, ensuring the protection of the ocean environment, amid contemporary environmental and climate challenges [3]. In HPHT deep wells, conditions can reach 103.5 MPa and 177 °C, which require intervention operations to ensure functionality [4].

These operations support equipment repair, maintenance, and fluid injection, extending service life and ensuring integrity, which boosts production and prevent accidents, such as oil leaks, that may harm the environment [5-8]. For this, subsea systems between the wellhead and intervention riser are used: the Lower Riser Package (LRP) for well control and the Emergency Disconnection Package (EDP) for cutting the intervention string and sealing the well (Figure 1) [9–11].

Received on 26 September 2025; revised 28 September 2025.
Address for correspondence: João Victor Carvalho de Mattos. Av. Orlando Gomes, 1845 - Piatã, Salvador – BA – Brazil, Zipcode: 41650-010. E-mail: arthur.azevedo@fbter.org.br.

J Bioeng. Tech. Health 2025;8(6):552-563

Figure 1 represents these systems, with accumulators and intervention panels; the EDP, located at the top, functions as an additional pressure barrier, while the LRP serves as the primary barrier, containing two main valves for wireline and coiled tubing cutting [12,13]. These systems, exposed to adverse conditions that may lead to failures, are essential for operational safety [14,16]. Efforts focus on improving efficiency and simplifying intervention system design to reduce costs and support deep-water oil production [17].

This study presents the initial phase of a structural sizing project for a forged EDP valve body for offshore HPHT wellheads, covering material selection, stress and dimension calculations, and a preliminary fatigue life analysis and finite element verification.

Theoretical Basis

The EDP may adopt various structural configurations, differing in cavity layout, shape, or shearing valve type. Figure 2 shows a linear-actuated valve for well sealing in operations up to 137.9 MPa, suitable for HPHT use. Its forged, unified structure protects internal components and mechanisms. Forging minimizes defects and

Figure 1. Positioning and structure of intervention systems [11,12].

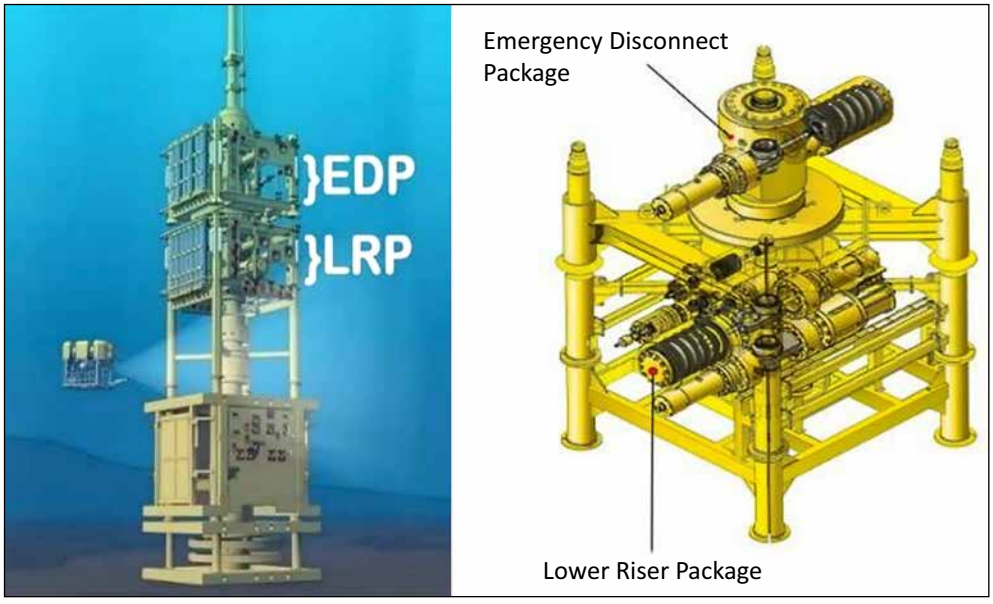

Figure 2. EDP valve body structure for intervention operations [17].

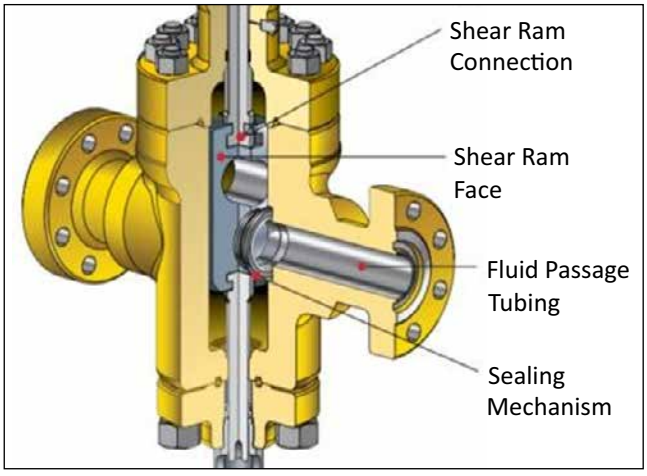

increases strength, with materials chosen for high mechanical and corrosion resistance [18-20]. Proper sizing is essential for safe interventions and to maintain production under critical conditions [4,13,18,21].

For HPHT analysis, API 17TR8 outlines key design and construction guidelines, addressing corrosion, fatigue, and plastic collapse [22–26].

Table 1 defines corrosion failure criteria, setting minimum H_2S concentrations for sulfide stress corrosion based on pressure [27]. At 103.5 MPa, H_2S above 2.5 ppm classifies the environment as sour, requiring metallurgical evaluation for operational viability [24].

At high temperatures, steels lose yield strength, requiring reduction factors in the design of bodies, flanges, and bolts [28–31]. Subsea equipment must comply with structural integrity standards [23]. This study applies API 17TR8's flowchart for 103.5–137.9 MPa and ASME VIII Divisions 2 and 3 [22]. Stress analysis follows Lamé's method for thick-walled cylinders [32], with allowable stresses from ASME II-D and VIII-2, and sizing features per API 6A [33-35].

Table 1. Minimum H_2S concentration for acidic environment classification [22].

Rated Working Pressure	69 MPa	103 MPa	138 MPa	172 MPa	207 MPa
Concentration of H_2S (ppm)	5	3.3	2.5	2	1.7

Fatigue is analyzed via stress cycling and fracture mechanics, crucial for HPHT conditions, supported by tests and statistical models [33,36–38]. Plastic collapse considers linear or elasto-plastic behavior, focusing on stress concentrators [33,39-41]. Testing validates designs but is costly, so modeling and simulations are used [19,25,33,42–45].

The Finite Elements Method (FEM), endorsed by API 17TR8, enables accurate, cost-effective simulations of complex geometries [22,26,40,46,47].

The aforementioned standards, despite being written by international organizations, are recognized by Brazilian corporations and agencies, being used and referenced for projects in the national territory [48-50].

Materials and Methods

The method defined design conditions, developed an analytical model for load, stress, and fatigue life, and applied FEM.

Design Conditions

Design pressure was 103.5 MPa, operating 51.8 MPa, and temperature 176.7 °C. based on 3000 m HPHT wells in Potiguar and Sergipe-Alagoas basins [1,51–55]. The analyses covered stress, deformation, fatigue, and hydrostatic tests [22,33].

An 11″ cylindrical shear valve body with two lateral holes (Figure 2) was sized analytically and numerically. Forged AISI 4145H steel, quenched and tempered, was the chosen material, for its acceptable hardness, nickel content, and corrosion resistance [27,56]. Its ambient yield strength is 862 MPa [57,58], reduced to 90% for high temperature, per API 6MET [28]. An API 6A integral flange (Figure 3), was selected based on the proposed pressure and dimensions [35,59].

The hub's vertical flange nominal diameter was set at 11'', and the side flange was 13 5/8'', to fit the shear ram. Tables 2 and 3 detailed flange and bolt sizes [35,59].

For fasteners, SA-320 Grade L7 material was chosen for subsea use, with required properties in

Figure 3. Flange 6A with BX seal for 103.5 MPa operating pressure [35].

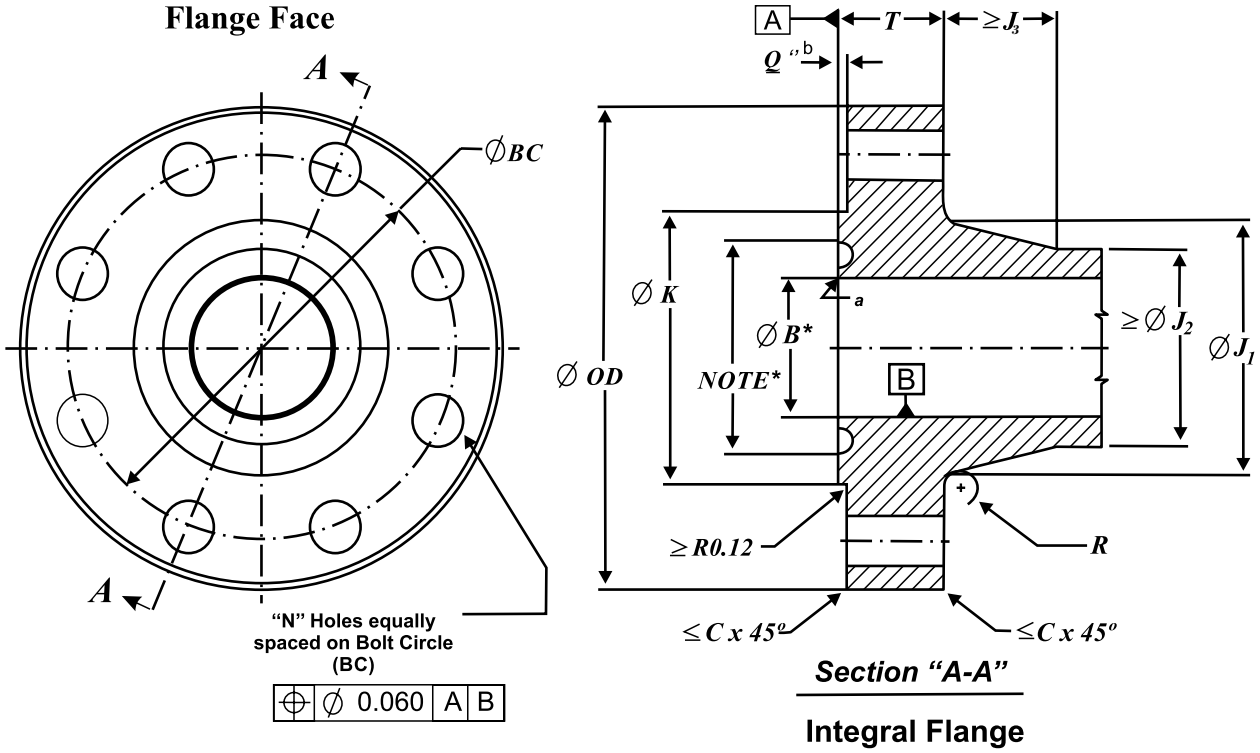

Table 2. Dimensions for API 6BX integral flanges to 103.5 MPa [35].

Normal size and Bore of Flange		Basic Flange Dimensions							
		Maximum bore	Outside diameter of flange		Maximum chamfer	Diameter of raised face	Total Thickness of flange	Large diameter of hub	Small-diameter of hub
(in)	(mm)	*B*	*OD*	tol.	*C*	*K* ± *1.6*	*T* + 3 0	*J₁* 0 -3	*J₂*
11	279	280.2	815	± 3	6	454	187.4	584.2	427.0
13⅝	346	346.9	885	± 3	6	451	204.8	595.3	528.6

Table 3. Bolt dimensions for API 6BX flanges to 103.5 MPa [35].

Normal size and Bore of Flange		Bolting Dimensions								
		Length of hub	Radius of hub	Diameter of bolt circle	Number of bolts	Diameter of bolt	Diameter of bolt holes		Minimum length of stud bolts	Ring number
(in)	(mm)	*J₃*	*R*	*BC*		*(in)*		*tol.*[e]	*L_{ssb}*	*BX*
11	279	235.7	16	711.2	20	2	54	+ 2.5	490	158
13⅝	346	114.3	25	711.5	20	2¼	61	+ 2.5	540	159

Table 4. Mechanical properties of ferritic materials for high-alloy fasteners [61].

Class and Grade, Diameter, in [mm]	Heat Treatment	Minimum Tempering Temperature, °F [°C]	Tensile Strength, min, ksi [MPa]	Yield Strenght, min, ksi [MPa] (0.2 offset)	Elongation in 2 in. or 50 mm, min, %	Reduction of Area, min, %	Handness, max
Ferritic Steels							
L7, L7A, L7B, LTC,L70, L71, L72, L73			125	105	16	50	321 HBW or 35 HAC
21/2 [65] and under[A]	quenched and tempered	1100 [593]	[860]	[725]			

Table 4 [29,60]. Suitable for bolts up to 2,5″ (65 mm), heat treated by quenching and tempering, it has 35 HRC hardness, 724 MPa yield strength, and 861,85 MPa tensile strength. A safety factor of 2.0 was applied, considered acceptable [33,34,60].

Allowable Stresses and Loads Calculation

Allowable stresses were set as the minimum yield or rupture ratio, with its respective factors, as shown in Equation 1 [32].

$$S_{adm} = mín\left(\frac{S_y}{1,5}; \frac{S_u}{2,4}\right) \quad (1)$$

Loads were estimated from body-fixing bolts and flange forces under pressure and sea current moments, according to Equations 2 and 3 [33].

$$M_o = abs[((H_D * h_D + H_T * h_T + H_G * h_G) * B_{SC} + M_{oe}) * F_s] \quad (2)$$

$$M_g = W_g * (C + G) * B_{SC} * F_s) * 0,5 \quad (3)$$

These body stresses was defined accounting for stress concentrators and secondary stresses, and

safety factors [33,34,62]. The stiffness index was calculated per Equation 4 [33].

$$J = \frac{52{,}14 * V * M}{L * E * K_R * h_o} \quad (4)$$

Analysis of Lamé and Secondary Stresses

Lamé stress analysis, using defined dimensions and corrosion allowance, computed wall thickness and stresses by Equations 5–7 [32].

$$\sigma_{rr} = \frac{(p_1 * {R_1}^2)}{{R_2}^2 - {R_1}^2} - \frac{{R_1}^2 * {R_2}^2}{r^2 * ({R_2}^2 - {R_1}^2)} * (p_1) \quad (5)$$

$$\sigma_{\theta\theta} = \frac{(p_1 * {R_1}^2)}{{R_2}^2 - {R_1}^2} + \frac{{R_1}^2 * {R_2}^2}{r^2 * ({R_2}^2 - {R_1}^2)} * (p_1) \quad (6)$$

$$\sigma_{zz} = \frac{(p_1 * {R_1}^2)}{{R_2}^2 - {R_1}^2} + \frac{F}{\pi * ({R_2}^2 - {R_1}^2)} \quad (7)$$

Equivalent stresses by von Mises criterion (Equation 8) included self-weight, thermal effects, and concentration factors [33,41,61].

$$\sigma'_{eq\_\theta max} = \sqrt{\frac{(\sigma'_{\theta\theta} - \sigma'_{rr})^2 + (\sigma'_{rr} - \sigma'_{zz})^2 + (\sigma'_{zz} - \sigma'_{\theta\theta})^2}{2}} \quad (8)$$

Fatigue Life Analysis

Fatigue life followed the modified Goodman criterion, with resistance limits, factors and stresses (Equation) 9 [40].

$$\frac{\sigma'_m}{S_{ut}} + \frac{\sigma'_a}{S_f} = 1 \quad (9)$$

Finite Elements Method

FEM model evaluated stress–strain response under complex loading and geometry, complementing analytical results [22,33].

Results and Discussions

The EDP was designed per load and dimensional requirements. Figures 4 and 5 show the main body and a full 3D CAD model, with external structure and an internal sealing section. The design features a vertical bore, for coiled tubing, and a horizontal chamber, with a ram that shears the tube and seals the system via O-rings.

To verify structural integrity, stresses in the nozzle opening regions were analyzed. Allowable stresses for flanges, bolts, and the EDP body at design (177 °C) and sealing (ambient) temperatures are presented in Table 5, with body and flange stresses being identical due to its material equivalence. The stress reduction due to temperature is responsible for the difference in stresses between the two temperature conditions.

Flange load calculations considered the bending moments induced by sea current forces, which increase stresses acting on the body, as calculated previously. Table 6 presents the resulting loads for each designed flange. Stress concentrators were then accounted for, and flange integrity was assessed.

Table 7 lists the safety factors for operating, sealing, hydrostatic test, and combined Table 4. Safety Factors for EDP Flange Design stress conditions for both flanges, calculated by dividing the material's allowable stress by the acting stresses, following ASME VII-2 criteria, also shown in Table 7. This standard considers the unit as the minimum value to ensure equipment integrity, applying safety parameters as constants in the calculations, being a usual practice at the oil and gas sector. Therefore, all safety factors calculated below were acceptable, above the recommended minimum limit of 1, indicating that the equipment, with the calculated dimensions and chose materials, can withstand the forces and stresses acting on it [33].

A flange stiffness index analysis also confirmed compliance, with values below 1 for both sealing and operating conditions.

In the Lamé stress analysis with the Von Mises criterion, considering secondary stresses, it was found that wall holes created stress concentrators exceeding design limits. To mitigate this, lateral projections were added to the hole region (Figure 8), sized so that their external surface extended beyond the stress concentration zone, preventing overload on the necks between projections and flanges.

The local thickness increase preserved structural integrity while reducing material and financial costs compared to increasing the overall body thickness. Table 8 presents the safety coefficients

Figure 4. Top (a), side (b) and front view with section cut (c) of the EDP body.

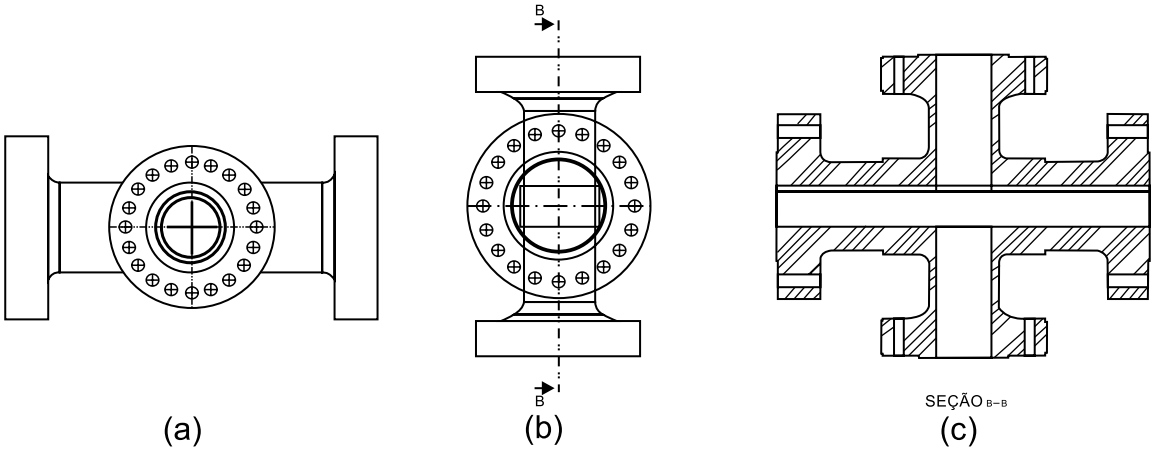

Figure 5. EDP CAD assembly.

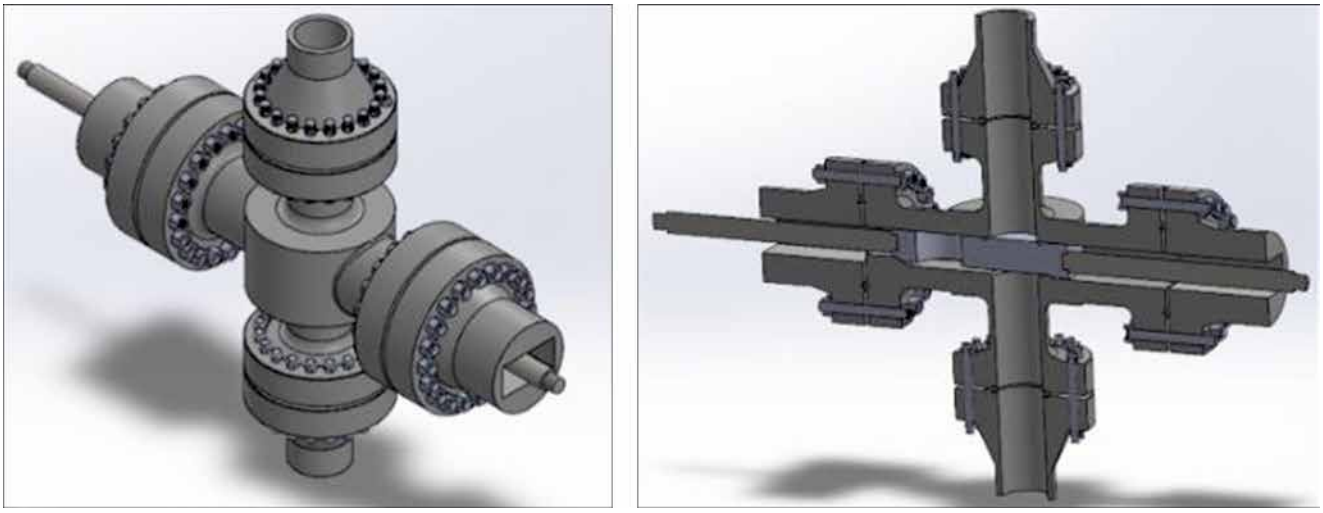

Table 5. Allowable stress for flanges and bolts.

Equipment Component	Allowable Stress at Design Temperature (MPa)	Allowable Stress at Sealing Temperature (MPa)
Body and Flanges	415,50	458.33
Flange Bolts	337.55	358.33

Table 6. Bending moment at flanges caused by current force.

Internal Diameter (In.)	Normal Force (N)	Shear Force (N)	Bending Moment (J)
11”	650	1166. 8	1.4E+5
13 ⅝”	650	1798.3	2.2E+5

Table 7. Safety factors for EDP flange design.

Component	Analyzed Condition	Calculation Method	Safety Coefficient
Axial Flange	Operation (With concentrator)	$\frac{1,5 * \sigma_{adm\_op}}{\sigma_{axial\_op} * K'_t}$	7,72
	Sealing (With concentrator)	$\frac{1,5 * \sigma_{adm\_sg}}{\sigma_{axial\_sg} * K'_t}$	5,80
	Hydrostatic Test (With concentrator)	$\frac{0,9 * S_{y\_Aço\_4145}}{\frac{P_{TH}}{P_i} * \sigma_{axial\_op} * K'_t}$	6,45
	Combination of Sealing Stresses (Axial + Tangential)	$\frac{2 * \sigma_{adm\_sg}}{\sigma_{axial\_sg} + \sigma_{tan\_sg}}$	8,57
	Combination of Sealing Stresses (Axial + Radial)	$\frac{2 * \sigma_{adm\_sg}}{\sigma_{axial\_sg} + \sigma_{radial\_sg}}$	4,75
	Combination of Stresses in Operation (Axial + Tangential)	$\frac{2 * \sigma_{adm\_op}}{\sigma_{axial\_op} + \sigma_{tan\_op}}$	11,40
	Combination of Stresses in Operation (Axial + Radial)	$\frac{2 * \sigma_{adm\_op}}{\sigma_{axial\_op} + \sigma_{radial\_op}}$	6,22
Side Flange	Operation (With concentrator)	$\frac{1,5 * \sigma_{adm\_op}}{\sigma_{axial\_op} * K'_t}$	9,03
	Sealing (With concentrator)	$\frac{1,5 * \sigma_{adm\_sg}}{\sigma_{axial\_sg} * K'_t}$	9,52
	Hydrostatic Test (With concentrator)	$\frac{0,9 * S_{y\_Aço\_4145}}{\frac{P_{TH}}{P_i} * \sigma_{axial\_op} * K'_t}$	7,55
	Combination of Sealing Stresses (Axial + Tangential)	$\frac{2 * \sigma_{adm\_sg}}{\sigma_{axial\_sg} + \sigma_{tan\_sg}}$	14,58
	Combination of Sealing Stresses (Axial + Radial)	$\frac{2 * \sigma_{adm\_sg}}{\sigma_{axial\_sg} + \sigma_{radial\_sg}}$	5,56
	Combination of Stresses in Operation (Axial + Tangential)	$\frac{2 * \sigma_{adm\_op}}{\sigma_{axial\_op} + \sigma_{tan\_op}}$	13,83

for regions with and without stress concentration, calculated as the ratio between the material strength and the acting equivalent stresses.

Structural modifications ensured the equipment body met acceptance criteria under internal pressure and secondary loads, being suitable for the proposed operating conditions.

Simplified finite element analysis using ⅛ symmetry and three mesh sizes (20 mm, 5 mm, 2 mm) showed satisfactory mesh quality (Figure 6). The Jacobian criterion, ideally near unity, ranged from 1.0 to 1.16 in critical regions like the internal nozzle surface, nozzle necks, and ram sliding nozzle concentrator, being within the 20% tolerance [63] and validating the mesh quality.

The FEM analysis identified the highest stress concentrations in the thinnest regions and areas with geometric changes, confirming these as critical structural points. Figure 7 presents the maximum stress values under the most demanding load case, the Hydrostatic Test, which remain below the material's yield strength.

Table 8. Safety coefficients for equipment pressure conditions.

Load Condition	Radial Stress (MPa)	Circumferential Stress (Mpa)	Axial Stress (MPa)	Von Mises Stress (MPa)	Calculation Method	Safety Coef.
Operation, away from the concentrator	103,4	238,6	76,9	296,4	$\frac{Y_f * S_y}{\sigma_{eq}}$	2,17
Hydrostatic Test away from the concentrator	155,1	330,0	87,4	420,1	$\frac{0,9 * S_y}{\sigma_{eq}}$	1,47
Operation with concentrator	103,4	476,3	21,1	528,6	$\frac{Y_f * S_y}{\sigma_{eq}}$	1,41
Hydrostatic Test with concentrator	155,1	609,4	3,4	698,8	$\frac{0,9 * S_y}{\sigma_{eq}}$	1,11

Figure 6. Division and mesh quality in the analyzed element.

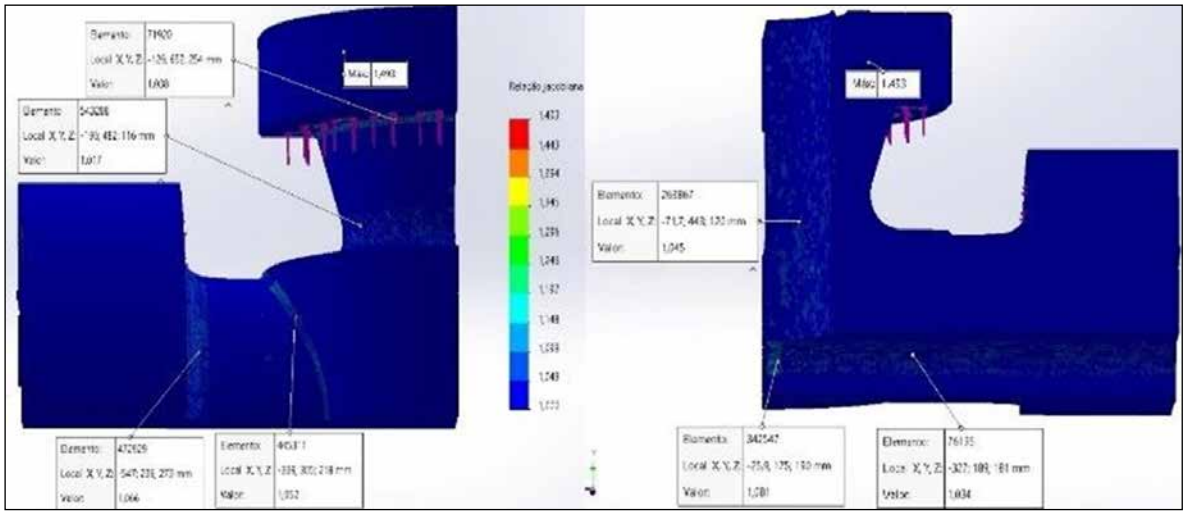

Figure 7. Von mises stress (hydrostatic test) on CAD model by FEM.

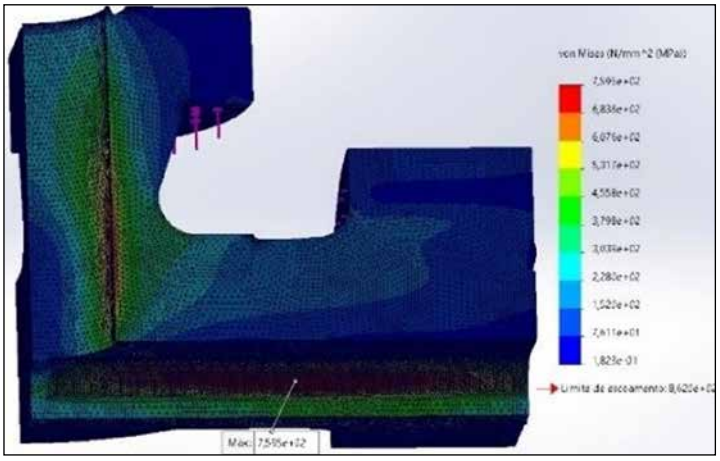

The analysis considered torque and bolt stress values recommended by API 6A for the respective types of flanges and bolts used in the equipment design [35]. Maximum stress zones extended along the flange necks, highlighting significant bending effects. Increasing thickness in these regions is a possible design optimization, to reduce those stresses and improve stiffness.

Based on the FEM results, safety coefficients were calculated for each analyzed scenario using the corresponding Von Mises stress values, as shown in Table 9. Differences between the numerical and analytical model results are attributed to FEM's consideration of complex factors excluded in the pressure vessel calculations, such as detailed geometric features, like angles, surfaces and cuts for ram movement.

Table 9. Safety coefficients based on stresses obtained by FEM.

Load Condition	Von Mises Stress (MPa)	Safety Coefficient
Operation	255.4	2.94
Project	507.6	1.54
Hydrostatic Test	759.5	1.02

Despite increased stress during the hydrostatic test, all safety coefficients remained within acceptable limits, corroborating the analytical results and indicating the equipment's suitability for the intended operations. However, both analytical and numerical results approached critical values under hydrostatic conditions, suggesting the need for structural optimization, particularly increasing wall thickness at the nozzle necks.

Additionally, membrane stresses on the equipment wall were analysed and compared between analytical and numerical methods using Von Mises stress at average wall thickness. Table 10 presents these stress values and corresponding safety coefficients, calculated as the ratio of membrane stress to the material's allowable stress.

Table 10. Safety coefficients based on membrane stresses obtained in FEM.

Type of Analysis	Load Condition	Membrane Stress (MPa)	Safety Coefficient
Analytical	Project	239.5	1.72
	Hydrostatic Test	353.3	1.30
Numerical (FEM)	Project	240.2	1.72
	Hydrostatic Test	363.2	1.27

The stress values obtained for this criterion were within acceptable limits and showed close between the analytical and numerical methods. Thermal stresses acting on the body under design conditions were also evaluated, combined with pressure effects, to assess combined stresses via FEM. Results, presented in Table 11, remained within acceptance limits, with higher maximum stresses compared to the pressure-only case due to the additional thermal loading.

Table 11. Combined stresses analysis by FEM.

Combined Stresses Case	Stress Value (MPa)	Safety Coef.
Von Mises Stresses	549.1	1.43
Maximum Stresses	571.3	1.43

The fatigue life analysis, yielded a safety factor of approximately 0.4, indicating that the equipment has a finite service life, operating up to 42756 cycles. This indicates less operating time than usual for those equipments and a need for earlier replacement. This is a topic that requires further analysis and refinement in later stages of this project, considering a change in materials or the changes in well pressure levels at different

stages of its life cycle, since production declines are natural in these structures, and these reduce pressure levels during operation [64].

The design assumptions and simplifications applied in the analyses effectively optimized computational resources and reduced calculation complexity without compromising result quality. The outcomes were consistent with each other and aligned with the theoretical framework, adequately representing the functionality of the modelled mechanisms and the structural integrity of the components.

Conclusions

The equipment was sized according to manufacturing and dimensional specifications, utilizing 11″ and 13⅝″ API 6BX flanges made from AISI 4145H steel. The objectives were successfully met, with both analytical and finite element analyses showing compliance within acceptable design limits. In the hydrostatic test, safety coefficients values are close to 1, indicating the need to increase wall thickness, in order to ensure integrity under critical conditions.

As expected, stresses during the hydrostatic test were notably higher than design stresses, due to increased pressure, and stress concentrators significantly amplified these stresses, which justifies careful consideration of this aspect in future design phases.

Fatigue life analysis indicated that the designed EDP valve operates over a finite life cycle, which is not recommended for this type of equipment. Therefore, a more detailed analysis, considering well pressure variations throughout its service life and material optimization, should be performed to achieve more appropriate results.

The development of such equipment is vital for advancing the oil and gas industry, ensuring well integrity and sustained production, particularly at the national level.

Results highlight the importance of accurately determining operating conditions to assess structural integrity, especially for subsea HPHT equipment where pressure is a critical factor influencing stresses.

Another potential improvement includes refining the CAD model with structural optimization and running FEM analysis in other software, as Ansys or Abaqus, to verify and confirm the results.

Acknowledgement

The team thanks SENAI CIMATEC University for providing computers, software and access to references necessary for the development of this study, as well as the team of professors and advisors for all the support given.

References

1. Petrobras. Bacia Sergipe-Alagoas: conheça as oportunidades, características e desafios dessa nova fronteira. Petrobras Nossa Energia; 2024. Disponível em:https://nossaenergia.petrobras.com.br/w/nossas-atividades/bacia-sergipe-alagoas-conheca-as-oportunidades.
2. Petrobras to present development plan for Sergipe deep waters by the end of April. Brazil Energy Insight; 2025. Disponível em: https://brazilenergyinsight.com/2025/04/03/petrobras-to-present-development-plan-for-sergipe-deep-waters-by-the-end-of-april/.
3. Hachem KE, Kang M. Reducing oil and gas well leakage: a review of leakage drivers, methane detection and repair options. Environ Res Infrastruct Sustain. 2023;3.
4. Skeels BH, Shanks EF, Hoshman MR. API 17TR8 – HPHT design guideline for subsea equipment: a focus on fatigue. In: Offshore Technology Conference; 2023.
5. Alaskar S, Alluqmani M. Well interventions: a reflection on the past and the present. J Pet Technol. 2023. Disponível em: https://jpt.spe.org/twa/well-interventions-a-reflection-on-the-past-and-the-present.
6. SLB. Well intervention: extending the life of producing wells. SLB; 2023. Disponível em: https://www.slb.com/products-and-services/innovating-in-oil-and-gas/well-intervention.
7. Trendsetter Engineering. Trident modular intervention system: technical information sheet. May 2022. Disponível em: https://www.trendsetterengineering.com/.
8. Ozowe C, Sofoluwe OO, Ukato A, Jambol DD. Future directions in well intervention: a conceptual exploration of emerging technologies and techniques. Eng Sci Technol J. 2024;5(5).

9. Expro. Expro helps customer to recover well by performing a through coiled tubing cut above stuck BHA. Disponível em: https://www.expro.com/case-studies/expro-helps-customer-to-recover-well-by-performing-a-through-coiled-tubing.
10. Bai Y, Bai Q. Subsea engineering handbook. 2nd ed. Oxford: Elsevier; 2019.
11. Expro Group. Intervention riser system. 2021. Disponível em: https://www.youtube.com/watch?v=AK9u7DOXji8
12. WOM Group. Subsea intervention systems. 2011.
13. WOM Group. WOM subsea capabilities brochure. 2022.
14. Norwegian Oil and Gas Association. Application of IEC 61508 and IEC 61511 in the Norwegian petroleum industry (recommended SIL requirements). NORSOK; 2020.
15. Liang X, Liu Z, Hung D, Wang T, Wang C. Experimental and numerical investigation of the drag coefficients of subsea tree. Ocean Eng. 2021.
16. SLB. The defining series: HPHT wells. 2016. Disponível em: https://www.slb.com/resource-library/oilfield-review/defining-series/defining-hpht.
17. HPHT: completions, challenges, and coping with the pressure. Oil and Gas IQ; 2019. Disponível em: https://www.oilandgasiq.com.
18. Legorburu J, Johnson K, Kerr S. Offshore oil and gas. 1st ed. Gistrup: River Publishers; 2018.
19. Interventek. Hydraulically operated compact shear and seal retainer valve designed with high cutting performance and reliable post-cut sealing. 2025.
20. WOM Group. WOM general catalog. 2015.
21. Sotoodeh K. Subsea valves and actuators for the oil and gas industry. Oxford: Elsevier; 2021.
22. Vargas A. Use of rotating control devices in high-pressure/high-temperature applications in Brazil provides economic and HSE benefits. In: Society of Petroleum Engineers Conference; 2006.
23. American Petroleum Institute. API technical report 17TR8: high-pressure high-temperature design guidelines. 2nd ed. Washington (DC): API; 2018.
24. Karpanan K, Kirkemo F. Structural capacity analysis of subsea equipment. 2024.
25. Yakoot SM, Valecillos ED. Strategic enhancement of well integrity in ultra-sour HPHT wells: a multidimensional approach. OnePetro. 2024 Nov.
26. Freeman M, White J. Assessment of failure modes of a rising stem type gate valve according to ASME BPVC Section VIII Division 2. SPE J. 2015.
27. Wang Y, Li Z, Luo W, Wang W, Yang J, Li J, et al. Fatigue life prediction method for subsea wellhead welds. Ocean Eng. 2022 Feb.
28. NACE MR0175/ISO 15156-1. Materials for use in H_2S-containing environments in oil and gas production. 1st ed. 2020.
29. American Petroleum Institute. API technical report 6MET: metallic material limits for wellhead equipment used in high temperature. 2nd ed. 2018.
30. Petrobras. Fixadores em aço baixa liga de alta resistência para aplicação submarina. ET-300000-1500-251-PEK-001-B; 2022.
31. Monteiro L, Junior R, Costa J, Ochoa A, Michima P. Assessment of failure modes of a rising stem type gate valve. Eng Fail Anal. 2024 Jul.
32. Boresi PA, Schmidt JR. Advanced mechanics of materials. 6th ed. Hoboken: Wiley; 2003.
33. ASME. Boiler and pressure vessel code, Section II, Part D. New York: ASME; 2019.
34. ASME. Boiler and pressure vessel code, Section VIII, Division 2. New York: ASME; 2023.
35. American Petroleum Institute. API 6A: specification for wellhead and tree equipment. 21st ed. 2018.
36. Kokurek C, Pathak P, Melancon C, Sohn S. Merging ASME and API design methods for subsea equipment up to 25,000 psi. In: Offshore Technology Conference; 2012.
37. Sahoo J, Campbell M, Cerkovnik M. Fracture mechanics based fatigue assessment of an HPHT valve body. In: Offshore Technology Conference; 2019.
38. Karpanan K, Skeels B. Fatigue analysis of HPHT subsea equipment according to API 17TR8. In: ASME PVP Conference Proceedings; 2024.
39. Wormsen A, Avice M, Fjedstad A, Reinas L, Macdonald K, Muff A. Base material fatigue data for low alloy forged steels. Int J Fatigue. 2015.
40. Pathak P, Kocurek C. Design methods combining API and ASME codes for subsea equipment. 2014.
41. Norton RL. Projeto de máquinas: uma abordagem integrada. 7ª ed. São Paulo: Bookman; 2013.
42. Budynas RG, Shigley JE, Mischke CR. Mechanical engineering design. New York: McGraw-Hill; 2008.
43. Wei P, Juan D, Tongyi Z, Zhiguo Q, Gang L. Well testing technique for HPHT sour gas wells in China. In: Offshore Technology Conference; 2015.
44. Schrank ABS, Santos TD, Altenhofen SD, et al. Interactions between clays and carbonates in Aptian pre-salt reservoirs. Geosciences (MDPI). 2024 Feb.
45. Chia B, Hemaprasertsuk J, Hamdan M, et al. Lessons learned from high-rate HPHT well testing campaign. In: IPTC; 2025.
46. Wu S, Zhang Q, Li B, Zhang L, Zheng W, Liu Y. Reliability analysis of subsea wellhead systems. Ocean Eng. 2023 Jul.
47. Bridge C. Subsea well intervention: spoolable compliant guide. 2010.
48. Petrobras. Technical specification for hard pipe. I-ET-3010.2D-1200-200-P4X-010; 2022.
49. Petrobras. Tie-in spool manufacturing. I-ET-0000.00-0000-24A-P9U-002; 2022.

50. American Petroleum Institute. API standards: international usage and deployment. 2022.
51. Werkle H. Finite elements in structural analysis. Springer; 2019.
52. Mosca F, Bruder N, Aasmyr H, et al. Thermal regime of deep-water Sergipe and Potiguar basins. In: AAPG Annual Convention; 2019.
53. Zembruscki S, Klant C. Gradiente geotérmico das bacias sedimentares brasileiras. Petrobras; 1989.
54. Petrobras. Petrobras discovers oil in ultra-deep waters of the Potiguar Basin. 2024. Disponível em: https://agencia.petrobras.com.br.
55. Silva A. Perfuração e completação de poços HPHT. Niterói: UFF; 2016.
56. Rodriguez K, Saunders M, Hodgson N, Geiger L. Sergipe Basin: undrilled potential surpasses giant offshore discoveries. Spectrum. 2017.
57. Yue C, Cai H, Kong L, Liang C. Wear behaviors of AISI 4145H drilling tool steel. 2022.
58. Sverdrup Steel. AISI 4145H modified / UNS G41450. 2024. Disponível em: https://www.sverdrupsteel.com.
59. Kondaiah V, Kumaran S. Experimental investigation on microstructural and mechanical properties of quenched AISI 4145 steel. Indian J Eng Mater Sci. 2019 Apr.
60. Carpenter C. A design combining API and ASME codes for subsea equipment in HPHT conditions. J Pet Technol. 2013.
61. ASTM International. ASTM A320/A320M: standard specification for alloy-steel and stainless steel bolting. 2017.
62. Pilkey W. Peterson's stress concentration factors. 2nd ed. Wiley; 2008.
63. SolidWorks Corporation. An introduction to stress analysis applications with SolidWorks Simulation. Student guide; 2010.
64. Wachtmeister H, Lund L, Aleklett K, Höök M. Production decline curves of tight oil wells. Nat Resour Res. 2017;26(3).